Research Article

Effect of Fe Concentration on the Properties of Zn-Fe-Mn Alloy Electrodeposited on a Low-Carbon Steel

Emad A. Matter, Gehan A. El-Naggar, Mahmoud A. Younis *, Ghada E. Abd Elgawad

Chemistry Department, Faculty of Science, Damanhour University, Egypt
Corresponding Author: mahmoudyounis@sci.dmu.edu.eg

Abstract

Zn-Fe-Mn coatings were electrodeposited galvanostatically at 25°C on low carbon steel from acidic sulfate baths (pH 2.3±0.2) consisting of $ZnSO_4.7H_2O$, $FeSO4.7H_2O$, $MnSO_4.H_2O$, Na_2SO_4, boric acid and ascorbic acid. The study was carried out using electrochemical methods such as cyclic voltammetry, galvanostatic deposition for electrodeposition and anodic linear sweep voltammetry, while linear polarization and electrochemical impedance spectroscopy techniques were used for the corrosion study. Structural analysis by X-ray diffraction (XRD) method revealed that the Zn–Fe–Mn alloys consisted of a mixture of zinc oxide, pure Mn, pure Zn, pure Fe and (Fe_3Zn_{10}) phases. Surface morphology and chemical composition of the deposits were also examined by using scanning electron microscopy and energy-dispersive X-Ray. It was found that the obtained Zn–Fe–Mn alloy with high Fe concentration exhibited a more preferred surface appearance and better corrosion resistance. Results obtained revealed that the increase in corrosion resistance of the ternary deposit can be attributed to iron co-deposition and the formation of (Fe_3Zn_{10}) phase.

1. Introduction

The co-deposition of zinc with other elements, on metal surfaces is performed to obtain coatings, which protect the substrate from corrosion. Among the elements co-deposited with Zn stand out those of group eight in the periodic table, especially Fe, Co and Ni. The Zn-Fe, Zn-Ni and Zn-Co alloys stand out in relation to the pure Zn because they confer better corrosion protection, superior weldability and formability [1,2]. The inclusion of Fe may result in Zn-Ni-Fe co-deposit with better protection against corrosion and formation of a more uniform surface compared to Zn-Ni, for example [3-5].

Another aspect characteristic of Fe^{2+} is its spontaneous oxidation to Fe^{3+}, which varies mainly with pH, depending also on other factors such as: concentration of this ion, time the solution remains at rest, dissolved O_2 and temperature [6-9]. Some authors add ascorbic acid (AA) in electrolytic solutions to avoid this oxidation [10-12].

The introduction of a third alloying element, with higher corrosion resistance and better physico-mechanical properties than that of zinc matrix, is another possibility. Mn has an electrically more negative potential (E° Mn/Mn^{2+} = -1.185 V vs. SHE) when compared to Zn. However, this alloy shows a synergistic effect with better corrosion resistance than the individual metals. In addition, the alloying elements are environmentally friendly. Zn–Mn alloy coatings, besides the fact that they are thermodynamically less noble than Zn, show a passivating behavior

under severely corroding environments due to the formation of insoluble compounds on the corroding surface that affect the catalytic activity for cathodic oxygen reduction [13,14].

To derive benefit from the advantages of Zn-Mn deposits, many efforts have been made to overcome the difficulties arising from the co-deposition of the alloying elements Zn and Mn. These difficulties arise from the following facts i): the large gap between the standard potentials of Zn (E° (Zn^{+2}/Zn) = -0.76 vs. SHE) and Mn (E°(Mn^{+2}/Mn) = -1.18 vs. SHE), ii) these two potentials are notably more negative than that of hydrogen evolution reaction, and iii) Zn-Mn coatings are obtained under the so-called normal co-deposition. This means that the electrodeposition of the less noble Mn is unfavored in comparison with Zn [15,16].

The purpose of this work was to study the feasibility of Fe co-deposition with Zn and Mn from an acidic Zn-Fe-Mn sulfate bath and to investigate the effect of various concentrations of Fe on the corrosion protection of Zn−Fe−Mn coatings. To the best of our knowledge, the bath compositions used in this study have not been reported before. The deposits were investigated by electrochemical techniques such as cyclic voltammetry, chrono potentiometry to electrodeposit the coatings galvanostatically and linear sweep voltammetry techniques. Linear polarization and electrochemical impedance measurements were used to evaluate the corrosion behavior of coatings in 3.5% NaCl solution. Moreover, X-ray diffraction (XRD) was used to characterize the phase structure of the coatings, scanning electron microscopy (SEM) was used to investigate the surface morphology of samples and Energy dispersive X-Ray (EDX) was used to identify the chemical composition of the coatings.

2. Materials and Methods
2.1. Chemicals and reagents
Ferrous sulfate heptahydrate from Alpha Chemika company (https://www.alpha-chemika.com/), zinc sulfate heptahydrate, manganese sulfate monohydrate and sodium chloride from El Nasr Pharmaceutical Chemicals company (https://elnasrpharma.com/), sodium sulfate anhydrous from Piochem Laboratory Chemicals company (https://piochem.com/), L-ascorbic acid (extra pure) from Oxford Lab Fine Chem LLP company (https://www.oxfordlabfinechem.com/), boric acid from El-Gomhouria company (https://el-gomhouria.com/en/), were all purchased to use in both the preparation and application processes. Distilled H$_2$O was used throughout the preparations and measurements. All commercial reagents were used without further purification.

2.2. The electrolytic bath
The main electrolytic bath used in the electrodeposition of Zn-Fe-Mn alloys has the composition (mol.L^{-1}): ZnSO$_4$.7H$_2$O-0.2; FeSO$_4$.7H$_2$O-0.2; MnSO$_4$.H$_2$O-0.2; Na$_2$SO$_4$-0.2; boric acid-0.2 and ascorbic acid-0.01. The electrolytic solutions were made fresh using double distilled water. All the solutions used in this study were produced and utilized without additional purification. The pH of the bath was determined to be 2.3 ± 0.2 using a Cyber Scan pH-meter Model 500 at 25°C ± 2°C. An acidic bath was used because it has a greater cathodic current efficiency. All tests were conducted in duplicate, and the reproducibility of these measurements was confirmed to be acceptable.

2.3. Substrates
(1) Low-carbon steel rod of area (0.503 cm^2) was used for electrochemical studies such as cyclic voltammetry, chrono potentiometry, electrochemical impedance spectroscopy, as well as anodic linear sweep voltammetry and linear polarization for electrodeposition of Zn, Fe, and Mn metals and their alloys. (2) A 1x1 cm^2 copper sheet was used for SEM and EDX measurements to eliminate the interference of iron from the steel substrate. Copper sheets were provided with a thin strip of approximately (1x0.4 cm^2) area to which clamp terminals for electrical contact were attached. A pure low-carbon steel rod with the chemical composition shown in Table 1. was acquired commercially.

Table 1: The chemical composition of the investigated low-carbon steel sample

Constituent	C	Si	S	P	Mn	Ni	Cr	Cu	Mo	Fe
Content (Wt. %)	0.28	0.23	0.048	0.018	0.73	0.10	0.08	0.45	0.017	Rest

2.4. Pretreatment of substrates

It was cut into cylindrical electrodes about 15 cm long. The electrodes were then placed on a Teflon mount such that just their cross-sectional area (0.503 cm^2) came into contact with the solution. As reference and counter electrodes, an Ag/AgCl electrode and a platinum electrode from Metrohm (https://www.metrohm.com/) were employed in all cases. The working electrode was mechanically polished using emery paper grades 400, 1800, 1200, and 1500, respectively. Therefore, a flat surface with a mirror finish was obtained. These electrodes were then cleaned with distilled water, dried, and immediately transferred to the cell after being treated with ethanol to eliminate residues of contaminants. Before each run, the surface was polished to a 1500 grade and washed.

2.5. Testing methods

In this study, Metrohm Autolab PGSTAT128N 12 V/800 mA Potentiostat / Galvanostat electrochemical cell Analyzer was used for the electochemical measurements. (Autolab N series, Serial no: AUT86580, Manufacture: Metrohm Autolab B.V., Utrecht, The Netherlands). The Autolab device is powered by a computer running Nova 1.11 software, which allows for data collecting and processing and is used to detect linear polarization (LP) and electrochemical impedance spectroscopy (EIS).

Electrochemical tests were carried out using a three-electrode electrochemical cell. A platinum electrode was used as a counter electrode and a silver/silver chloride electrode (Ag/AgCl) as a standard electrode. Throughout the operation, the WE was kept at similar distances from both the reference and counter electrodes. Cyclic voltammetry experiments were initiated at -0.3 V in a negative direction and reversed at -1.2 V in a positive direction to -0.3 V at a scan rate of 5 mV s^{-1}. The galvanostatic measurements (Chrono potentiometry) were performed by keeping the current at a constant level of 10.0 mA cm^{-2} for 20 minutes. The Anodic Linear Sweep Voltammetry (ALSV) was carried out to complement the characterization of the coatings. The alloys were stripped at 25ºC and anodic potential from -1.3 to 0.0 V with a sweep rate of 5 mV s^{-1} in the same electroplating bath.

Corrosion measurements were performed in 100 mL of non-deaerated 3.5% NaCl solution with a neutral pH. Linear polarization (LP) measurements were carried out by anodically dissolving the coating using a potential from -0.8 V to 0.0 V with a scan rate of 5 mV s^{-1}. Electrochemical impedance spectroscopy (EIS) measurements were realized by applying an alternating perturbation within the frequency spectrum 10^{-4}-10^{-2} Hz using a sine wave of 10 mV.

Structure and morphology examination of the deposits were also accomplished. The X-ray diffraction patterns of deposits obtained were recorded with CuKα radiation (λ=1.54060 Å) of a Bruker D8 Discover Diffractometer, Germany. at 30 kV and 10 mA. The 2 theta angle (2θ) ranged from 10° to 70° at a scan rate of 0.04° per second. Concentrations of alloying elements in the deposits were measured by EDAX (Genesis) Energy Dispersive X-ray Analyzer, USA. The morphology of the deposits was examined using (FE-SEM) (QUANTA FEG 250 instrument, Netherlands) with an accelerating voltage of 20.00 kV at 1000x and 10.000x magnifications.

3. Results & Discussion

3.1. Electrochemical and impedance measurements

The cyclic voltammograms are a convenient spectrum-like diagram depicting the various phases that are exposed during the corrosion of the deposit [17]. So, the voltammetric technique was used to give information about the general behavior of varying Fe^{2+} concentration in the deposition process. The influence of Fe^{2+} concentration in the electrolyte on the cathodic polarization part of the cyclic voltammograms was studied. From Fig. 1., the potential jumps were performed from -0.3 V and reversed to a more positive potential at -1.2 V. In the cathodic part, it was reported that the deposition of Mn starts below -1.6V vs. Ag/AgCl and that for Zn and Fe occurs at -1.1V, -950V,

respectively [18,19], but in the current work, a single cathodic peak only appeared at approximately -1.14V, which can be attributed to the reduction of zinc. R. P. Oliveira et al. studied the electrodeposition of Zn-Ni-Fe alloy on low-carbon steel in the presence of Ascorbic acid as an antioxidant and reported that there was no formation of the cathodic peaks that precede the deposition process of the alloys when the solution to obtain Zn-Ni-Fe was prepared immediately before the test [20]. The parasitic reaction of hydrogen evolution occurs simultaneously with metal reduction and drastically increases the cathodic current density. This also plays a role in masking reduction peaks [21].
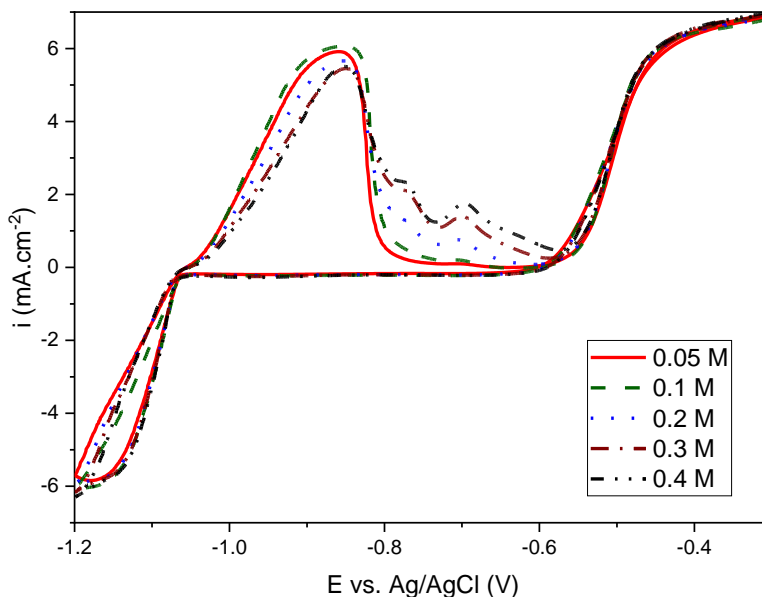

Figure 1: Cyclic voltammetry using the solutions immediately after preparation to obtain Zn-Fe-Mn deposits at various Fe concentrations at a scan rate of 5 mV.s^{-1} and 25 °C

For 0.05M, 0.1M and 0.2M, the cyclic voltammetry curves show two anodic peaks. The first peak appears at -0.86 V, which could be attributed to the dissolution of zinc from ZnO and pure Zn. The height of this peak decreases with increasing Fe^{2+} concentration in the plating bath. The second anodic peak at -0.69V represents the dissolution of free Fe. But for 0.3M and 0.4M, CV curves show three distinct anodic peaks, the first peak occurs at -0.85V and it is likely to represent the dissolution of zinc from ZnO and pure Zn phase. The second peak appears as a shoulder located at -0.77V and represents the dissolution of zinc from the Fe_3Zn_{10} phase. This finding is in agreement with the general rule according to which the deposition potential of an alloy (of an intermetallic compound or a phase) stands usually between those of the alloying elements taken separately [22]. The last anodic peak is located at -0.69V and it may represent the dissolution of pure Fe. Generally, the study of Mn electrodeposition is complicated by the fact that oxidation peaks of Mn are absent due to the instability of Mn deposits on steel substrates and their rapid dissolution in acidic media upon anodic sweep. A similar behavior was reported in the literature [19,23,24,25]. It should be noted that the dissolution of Mn is considered a non-faradic process [25,26]. On the other hand, the fact that the potential at which the dissolution begins is practically closer to that of the beginning of deposition indicates that the reduction process is reversible. The same finding has been reported by other authors [27-29].

Moreover, the results show a gradual decrease of both Zn content and cathodic current efficiency with increasing the concentration of Fe, this may be attributed to hydrogen evolution on the cathode surface. The deposition potentials of Zn are slightly shifted towards more negative values while those of Fe potentials are shifted positively.

In the nucleation process of galvanostatic electrodeposition, there is a gradual increase in cathodic deposition potential that can be attributed to the increase in Fe content and the presence of Zn and Mn. It is clear from Fig. 2. that co-deposition at 0.05M Fe needs low overpotential to create the initial nucleus, and by proceeding from 0.05M

to 0.4M, more overpotential is required. the galvanostatic curves are shifted towards the cathodic direction which may be ascribed to the increase in the Fe amount in the deposited alloy [30]. As the time increases in the 0.05M curve, the potential moves to more positive values till 451.8s, then the alloy grows at nearly a constant value of potential of -0.45V. The constant values of potential mean that there was not a significant modification in the characteristics of the alloys deposited on the electrode surface during the growth process. For 0.1M, 0.2M and 0.3M, the curves exhibit a similar deposition profile. However, the deposition at 0.4 M presents a different profile compared to other curves as there is a gradual potential reduction at approximately 1054s till the end of the growth process. This gradual increase in overpotential for the alloy indicates a decrease in the substrate area available for the transfer of cations in solution or an impediment of the diffusion of ions along the electrodeposition process at high concentrations of Fe [31]. It is very clear from the same figure that the nucleation time (t_N) reduces as the Fe content increases meanwhile the nucleation potential (E_N) shifts to more electronegative values. This refers to that more overpotential is needed to create the initial nucleus as Fe content increases.
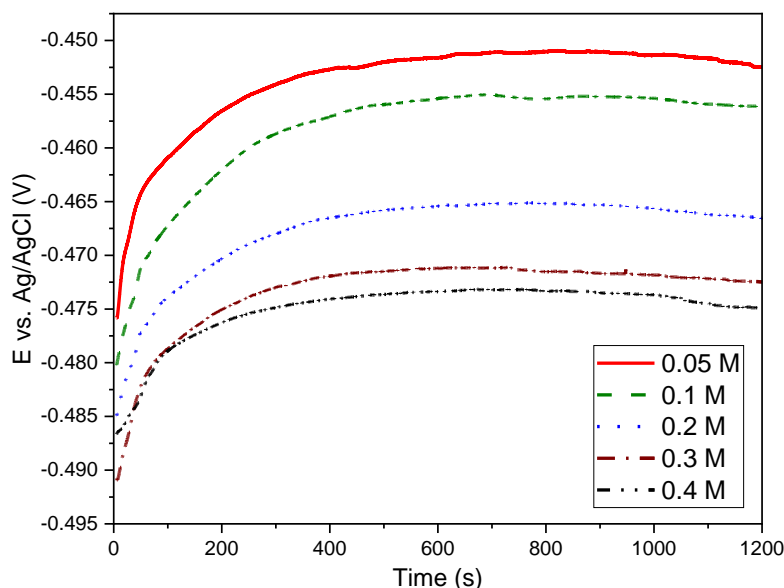

Figure 2: Galvanostatic electrodeposition curve of Zn-Fe-Mn at different concentrations of Fe at 10 mA cm^{-2} for 20 min

It is known that stripping methods such as anodic linear sweep voltammetry are useful to determine the chemical and phase compositions of the alloys. In case of Zn-Fe-Mn alloy, various peaks are observed in the oxidation scan that have been previously identified. The anodic linear sweep voltammograms obtained during the dissolution of the deposits show the influence of Fe^{2+} concentration on the phase structures of deposited Zn-Fe-Mn alloys (Fig. 3.). At a relatively low concentration of Fe (0.05M), the first dissolution peak at -0.89V representing the dissolution of zinc from ZnO and pure zinc has the highest intensity indicating a high amount of Zn in the deposit, but the second one at -0.7V representing Fe-rich phase is short indicating a lower percentage of Fe in the deposit. This is understood from the comparison between the heights of the peaks with each other as the size of the peaks indicates the amount of the phases in the coatings. This comes in good accordance with the results of EDX. Dissolution peaks for 0.05M, 0.1M and 0.2M Fe show the same behavior. But raising the concentration of Fe (to 0.3M and 0.4M) leads to more decrease in the height of the first dissolution peak appearing at -0.9V, corresponding to a more decrease in the content of pure Zn in the deposit. However, a shoulder appeared at approximately -0.78V, likely leading to the formation of more Fe content in the Fe_3Zn_{10} phase. An increase in the oxidation of iron can be understood from increasing the height of the third dissolution peak. Moreover, dissolution peaks are slightly shifted to a more positive potential, obtaining an overall deposit with good adhesion and corrosion resistance.
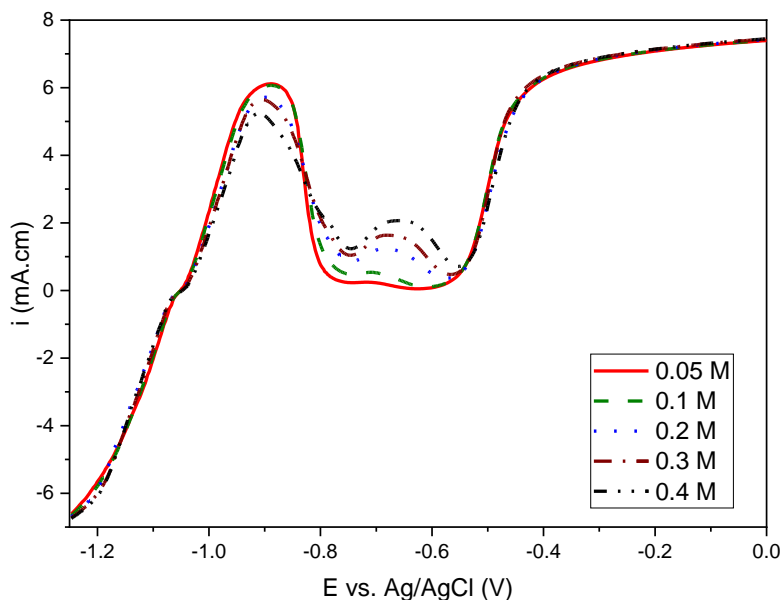
Figure 3: ALSV of the Zn-Fe-Mn deposits obtained by galvanostatic electrodeposition on low-carbon steel substrate at 25 °C and 5 mV.s⁻¹

It is noteworthy that Mn does not exhibit anodic peaks during the dissolution of the alloy. This may be ascribed to the low content of manganese in the deposited alloys with respect to the content of zinc and iron, which was approved by EDX analysis. Therefore, the manganese anodic peak may overlap with the anodic peak of the pure zinc phase. The low content of manganese can also be attributed to its high electronegative deposition potential with respect to the deposition potentials of zinc and iron [30]. ALSV experiments did not give unequivocal information about the correlation between plating bath composition and the phase structure of ternary Zn–Fe–Mn alloy coatings. Therefore, coatings deposited in the same conditions were submitted to the X-ray diffraction analysis.

Linear polarization measurements are used to determine the barrier resistance of the coatings by measuring the corrosion current density. Table 2. shows the current density, as well as other parameters that indicate the coatings oxidation rate, such as ba, bc, corrosion rate and polarization resistance measured using Tafel extrapolation techniques. At 0.05M, the corrosion potential (E_{corr}) at the beginning was -696 mV, which moved slowly towards a more positive value (more noble potential) by increasing the concentration of Fe in the coating bath (Fig. 4.). It was observed that as the concentration of iron increases, the concentration of zinc decreases. So, the decrease in E_{corr} may be ascribed to the increase in the concentration of the nobler element (Fe) that has a lower overpotential.

Table 2. Electrochemical corrosion parameters of LP for samples of Zn–Fe–Mo alloy coatings deposited at different Fe concentrations

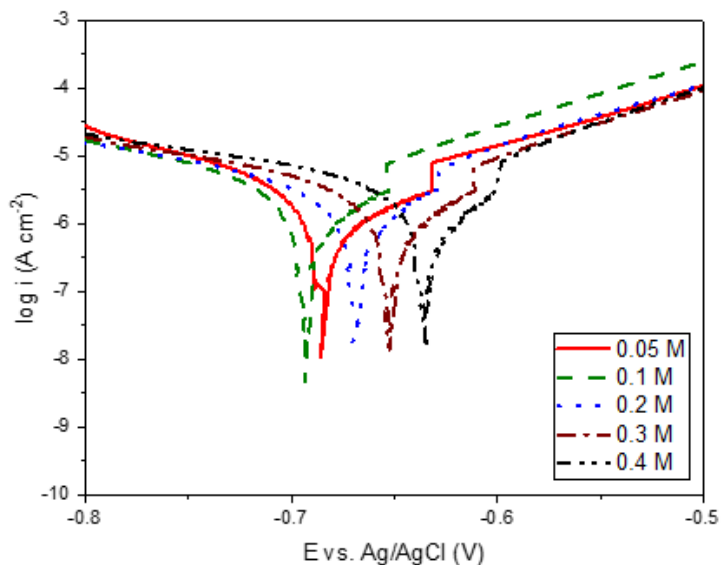| Parameters	Co-deposits				
	0.05 M	0.1 M	0.2 M	0.3 M	0.4 M
b_a (mV dec⁻¹)	113.61	82.7	79.38	63.96	22.8
b_c (mV dec⁻¹)	80.42	60.44	35.66	37.25	38.29
E_{corr} (mV)	-696	-688	-671	-653	-636
i_{corr} (μA)	2.04	1.48	0.77	0.65	0.37
Corrosion rate (mm/year)	0.024	0.017	0.009	0.007	0.004
Polarization resistance (kΩ)	9.99	10.21	13.87	15.55	16.94

Figure 4: Linear polarization curves of the Zn-Fe-Mn coatings at various Fe concentrations in 3.5% NaCl at 25°C

It is clear that the corrosion current density (i_{corr}) was slightly decreased with raising Fe concentration, this may be attributed to hydrogen evolution or to a sharp decrease in zinc and manganese deposition efficiency. These results are in agreement with those reported by Ashassi-Sorkhabi et al. and Abou-Krisha et al. [5,32]. Also, the polarization resistance of the deposit increased with increasing Fe content in the alloy, but the corrosion rate decreased. Thus, a more corrosion-resistant alloy could be obtained.

Electrochemical impedance measurements were used to evaluate the barrier properties of the coatings and to determine the polarization resistances without damaging the coatings. Fig. 5. represents a comparison of Nyquist responses obtained for different concentrations of Fe^{2+} alloys in 3.5% NaCl solution, where Z' and Z'' are the real and imaginary parts of the measured impedance, respectively. A qualitative analysis of the incomplete semi-circles shows the significantly higher impedance and larger diameter in the capacitive loops that reflect the higher corrosion resistance as the concentration of Fe increases from 0.05M to 0.4M in the coating. The spectra recorded for different concentrations of Fe were modeled by the classic Randle's cell, [R(Q[R(QR)])]. That was evidence of the presence of diffusion processes [33]. The equivalent circuit, shown in Fig. 6., was used to fit the EIS results, and the values of the equivalent circuit elements obtained by simulation using Nova software 1.11 are presented in Table 3.
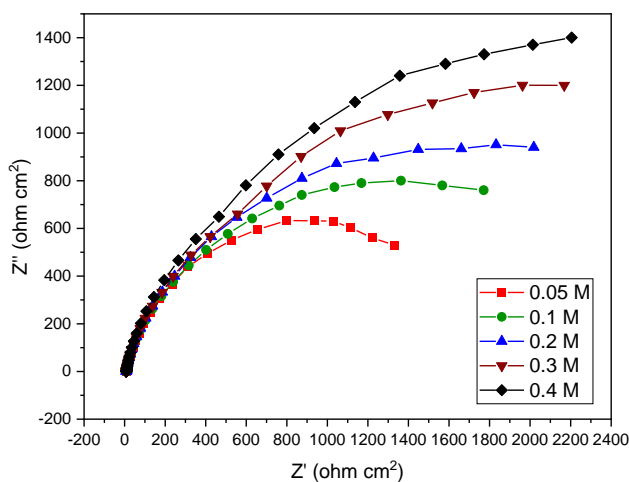

Figure 5: The electrochemical impedance curves for Zn-Fe-Mn coatings deposited galvanostatically at different Fe concentrations at 25°C
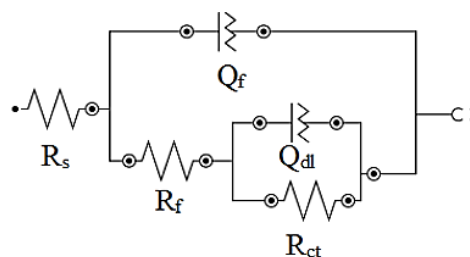
Figure 6: Electrical equivalent circuit used to fit EIS data recorded on a Zn-Fe-Mn coating deposited on a low-carbon steel electrode immersed in 3.5% NaCl solution at 25 °C

Table 3: The electrochemical impedance parameters for Zn-Fe-Mn coatings deposited galvanostatically at different Fe concentrations on a low-carbon steel electrode immersed in 3.5% NaCl solution at 25°C

Codeposits	R_s ($\Omega.cm^2$)	R_f ($K\Omega.cm^2$)	Q_f ($\Omega^{-1}.cm^{-2}.S^{-n}$) Y0 (mMho)	n	R_{ct} ($K\Omega.cm^2$)	Q_{dl} ($\Omega^{-1}.cm^{-2}.S^{-n}$) Y0 (mMho)	n	X^2	R_p ($K\Omega.cm^2$)
0.05M	8.73	1.22	2.02	0.861	1.30	5.50	0.651	0.1408	2.52
0.1M	8.62	1.25	1.14	0.875	1.89	5.34	0.775	0.0307	3.14
0.2M	7.84	1.30	1.03	0.868	2.57	4.36	0.752	0.0327	3.87
0.3M	7.63	1.98	1.44	0.851	3.07	3.20	0.598	0.1302	5.05
0.4M	8.35	2.10	1.91	0.887	3.26	3.12	0.701	0.0715	5.36

The experimental and calculated data matched well, indicating that the equivalent circuit was suitable for simulation. R_s is the resistance of the electrolyte between the electrodes determined by the conductance of the NaCl solution and according to these results, the solution resistance of all coatings shows no significant difference. R_f and constant phase element (Q_f) may be assigned to the electrolytic resistance in the pores and discontinuities of the film of corrosion products and the pseudo-capacitance of the porous corrosion products layer. R_{ct} is the charge transfer resistance and Q_{dl} is the double layer pseudo capacitance. The total polarization resistance (R_P) is the sum of R_f and R_{ct} i.e. $R_P = R_f + R_{ct}$ [34].

An analysis of the Nyquist plot shape (Fig. 5.) and the calculated values of CPE parameters presented in Table 2 (n – an exponent of a pseudo-capacitance) revealed that in all cases 0.5<n<1, meaning that the surface of samples was in non-homogenous status, this may be attributed to the complex electrochemical processes. Thus, instead of capacitances, constant phase elements (Q_f, Q_{dl}) have been used in the equivalent circuit [35,36]. The gradual increase in Fe concentration in the bath led to an increase in the values of R_f and R_{ct} and a decrease in Q_{dl}, confirming the superior anticorrosion property of the developed ternary Zn-Fe-Mn alloy deposit. Tables 3.1 and 3.2 compare the polarization resistance values of different Zn–Fe–Mn alloys calculated using linear polarization techniques and impedance analysis. The polarization resistance values obtained using EIS analysis are in good agreement with those obtained using linear polarization studies showing that both methods were reliable in confirming the improved corrosion resistance of the metallic coatings.

The total R_P values were calculated from the Nyquist plot and plotted against different concentrations of iron (0.05, 0.1, 0.2, 0.3 and 0.4 mol.L^{-1} FeSO$_4$·7H$_2$O). Fig. 7. shows that the R_P values of Zn-Fe-Mn coating increase with iron. The iron present in the plating bath has a considerable effect on increasing the iron content of the deposit. With an increase in the iron content of the deposit, resistance to the dissolution of zinc from the coating surface increases and the deposit becomes more noble. Thus, the increase in iron content of the deposit improves the corrosion resistance of developed Zn-Fe-Mn coating at different concentrations of iron in the plating bath.
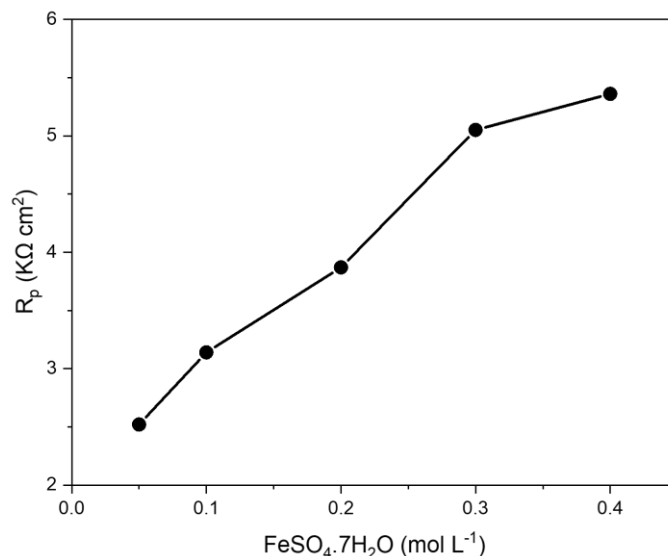
Figure 7: Total polarization resistance (RP) values of Zn-Fe-Mn deposit obtained galvanostatically at different Fe concentrations on a low-carbon steel electrode immersed in 3.5% NaCl solution at 25°C

3.2. Chemical Composition and morphological measurements

Fig. 8. shows the diffractogram of Zn–Mn–Sn coatings electrodeposited from 0.2M Zn–0.2M Mn–0.4M Fe electrolytic bath. The figure shows the presence of two diffraction peaks for Mn at 19.72° and 22.34°, one diffraction peak for ZnO at 34.02° [37], three diffraction peaks at 35.22°, 40.31° and 55.47° For Zn, two diffraction peaks that represent iron at 44.35° and 65.12° and three diffraction peaks for the Fe_3Zn_{10} intermetallic phase at 44.85°, 47.33° and 53.09°. The presence of the Fe_3Zn_{10} intermetallic phase increases the quality and anti-corrosive properties of the Zn-Fe-Mn intermetallic coating on low-carbon steel.
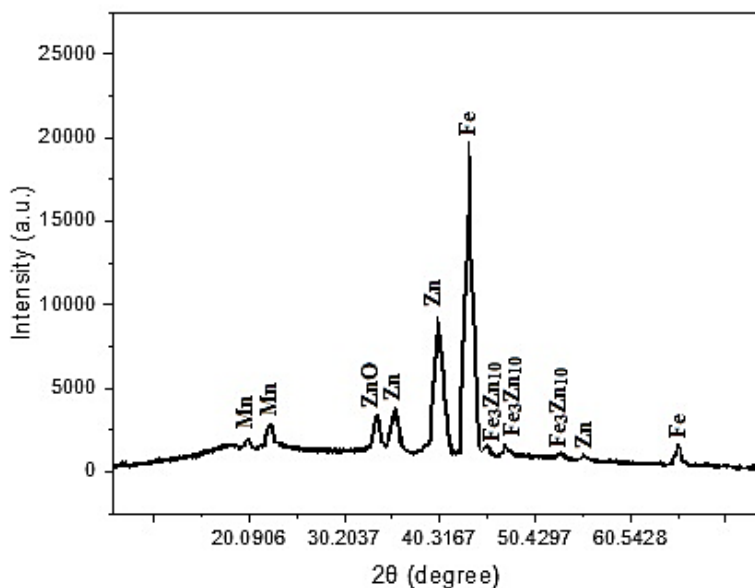

Figure 8: XRD pattern for Zn-Fe-Mn alloy electrodeposited at a high Fe concentration (0.4M) on a low-carbon steel electrode at 25°C

Fig. 9. shows the energy-dispersive X-Ray pattern of the deposit containing Zn–Fe–Mn alloy. A Cu substrate was used as WE during the deposition process in Chrono potentiometry to avoid the interference of iron from the steel

substrate. It can be seen from the peaks in this figure that zinc is the most readily deposited metal, under the conditions employed, and the deposition of ternary Zn-Fe-Mn alloys is of anomalous type. This is because the content of zinc in the deposit is always higher than its metal ion ratio in the solution [38,39]. According to previous work, [3,39,40] anomalous co-deposition behavior is attributed to the formation of zinc hydroxide film on the cathode surface due to hydrogen reduction, which suppresses the discharge of iron and manganese ions in the deposition of Zn-Fe-Mn alloys. In the present work, anomalous co-deposition may be due to the competitive adsorption between Zn^{2+} and/or Fe^{2+} and/or Mn^{2+} to occupy active sites leading to the preferential deposition of Zn.

Element	Weight %	Atomic %	Error %
MnK	2.1	2.48	37.23
FeK	2.86	3.32	25.65
ZnK	95.04	94.21	4.62

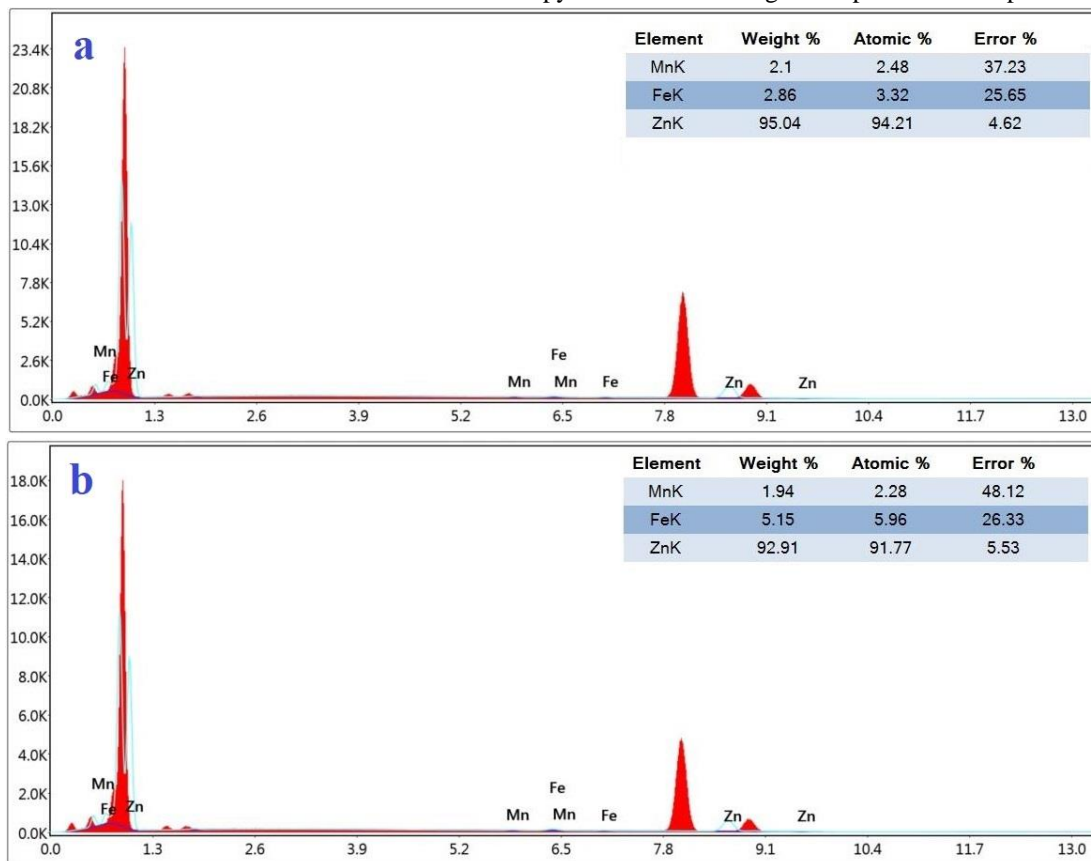| Element	Weight %	Atomic %	Error %
MnK	1.94	2.28	48.12
FeK	5.15	5.96	26.33
ZnK	92.91	91.77	5.53

Figure 9: EDX peaks for Zn-Fe-Mn alloys electrodeposited on a copper sheet from a bath containing 0.2M Na_2SO_4, 0.2M boric acid, 0.01M ascorbic acid and a) 0.2M Zn-0.2M Fe-0.2M Mn, b) 0.2M Zn-0.4M Fe-0.2M Mn at 25°C

As the concentration of iron increases in the electrolytic bath, the amount of zinc and manganese in the deposit decreases, which agrees with the observations of CV.

Slight changes in the structure and morphology can be observed from the scanning electron microscopy analysis. Fig. (10.a-d) shows the surface morphology of Zn-Fe-Mn electrodeposits at different Fe^{2+} concentrations. The Zn-Fe-Mn deposits at 0.2M Fe showed rough, non-homogenous structure and no uniform growth of the deposits grains; as shown in Fig. (10.a,b). However, at 0.4M Fe, the ternary Zn-Fe-Mn deposits show a slightly more homogenous structure form of crystallites, a more compact and more coherent deposit in contrast to that of 0.2M Fe, as shown in Fig. (10.c,d).
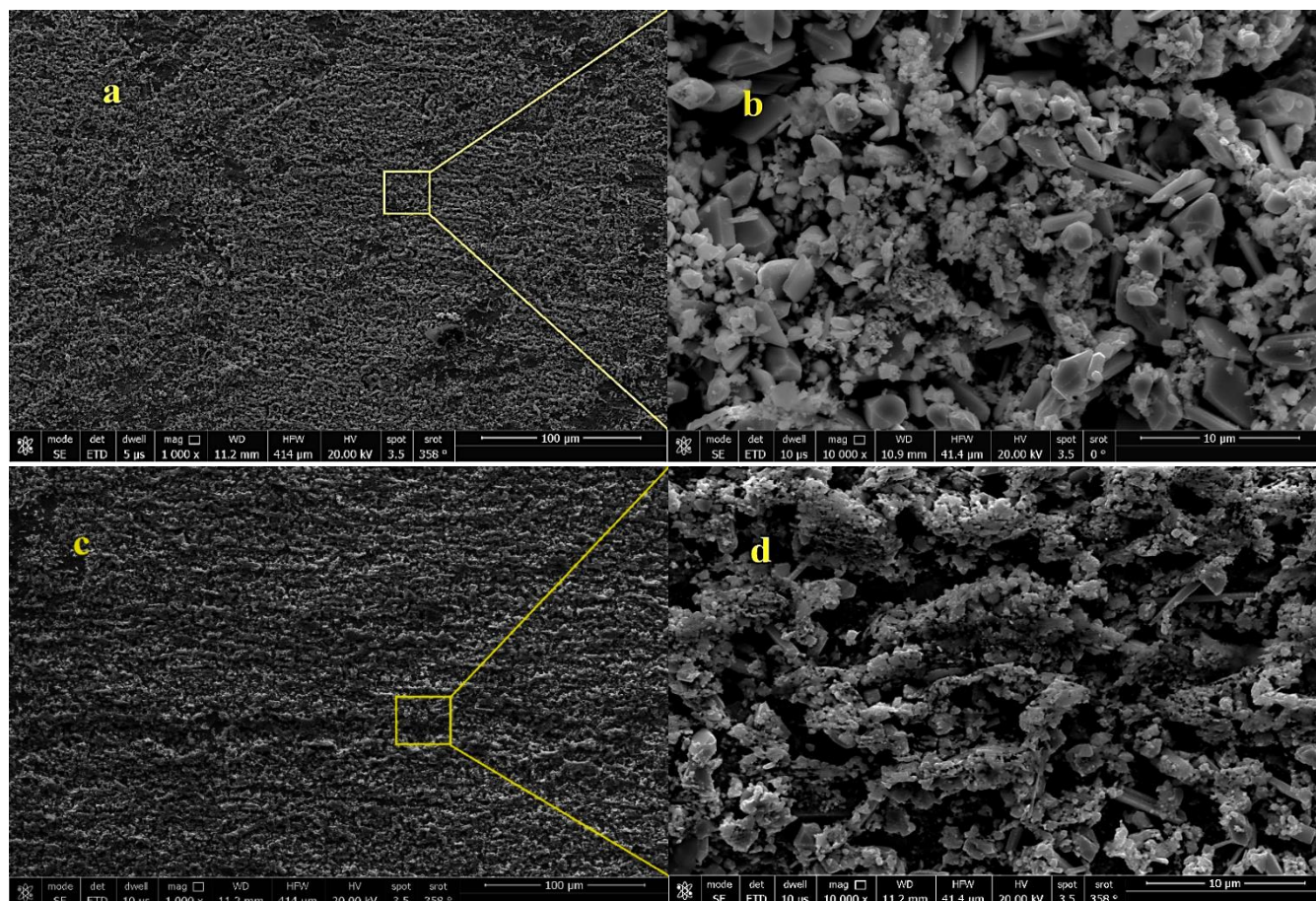
Figure 10: SEM photographs of electrodeposited Zn-Fe-Mn alloys on low-carbon steel from a bath containing 0.2M Zn-0.2M Fe-0.2M Mn a) at low magnification, b) at high magnification and another bath of 0.2M Zn-0.4M Fe-0.2M Mn c) at low magnification, d) at high magnification in presence of 0.2M Na$_2$SO$_4$, 0.2M boric acid, 0.01M ascorbic acid in all cases at 10 mA cm^{-2} for 20 min at 25°C

Conclusion

In summary, the following conclusions can be drawn from the presented results:

1. At high concentrations of Fe (more than 0.2M) electrodeposited with Zn and Mn, Fe$_3$Zn$_{10}$ phase is formed, which contributes to the enhanced corrosion resistance of the ternary alloy.

2. The chemical composition of the coatings changes by increasing the concentration of Fe. Co-deposition of Fe causes a decrease in the Zn and Mn amounts in the coating, which leads to the shift of corrosion potential towards more noble values.

3. By increasing the Fe content in the alloy, a slightly more homogenous, more compact and more coherent deposit can be obtained.

4. From linear polarization measurements, the values of i$_{corr}$ and E$_{corr}$ gradually decrease, while that of polarization resistance increases with increasing the concentration of Fe, which means the formation of more corrosion-resistant alloys.

5. From electrochemical impedance measurements, the gradual increase in Fe concentration in the bath leads to an increase in the values of R$_f$ and R$_{ct}$ and a decrease in Q$_{dl}$, confirming the superior anticorrosion property of the developed ternary Zn-Fe-Mn alloy deposit.

References

[1]. El Hajjami, A., et al. (2007). Appl. Surf. Sci., 254 480.

[2]. Bajat, J. B., Miskovic-Stankovic, V. B., & Kacarevic-Popovi, Z. (2003). Prog. Org. Coat., 47, 49.

[3]. Younan, M. M., & Oki, T. (1996). Electrodeposition of Zn-Ni-Fe alloy in acidic chloride bath with separated anodes. J. Appl. Electrochem., 26, 537–541.

[4]. Younan, M. M., Fadali, O. A., Aly, I. H. M., & Oki, T. (1996). Polarization phenomena during Zn-Ni-Fe alloy electrodeposition in acid chloride bath. Mater. Trans., 37, 1763–1767.

[5]. Abou-Krisha, M. M., Assaf, F. H., & El-Naby, S. A. (2009). Electrodeposition and characterization of zinc-nickel-iron alloy from sulfate bath: influence of plating bath temperature. J. Solid State Electrochem., 13, 879–885.

[6]. Stumm, W., & Morgan, J. J. (1996). Aquatic Chemistry: Chemical Equilibria and Rates in Natural Waters, third ed., John Wiley & Sons, New York.

[7]. Morgan, B., & Lahav, O. (2007). The effect of pH on the kinetics of spontaneous Fe(II) oxidation by O_2 in aqueous solution-basic principles and a simple heuristic description. Chemosphere, 68, 2080–2084.

[8]. Millero, F. J. (1985). The effect of ionic interactions on the oxidation of metals in natural waters. Geochim. Cosmochim Acta, 49, 547–553.

[9]. Millero, F. J., Sotolongo, S., & Izaguirre, M. (1987). The oxidation kinetics of Fe(II) in seawater, Geochim. Cosmochim. Acta, 51, 793–801.

[10]. Chitharanjan Hegde, A., Venkatakrishna, K., & Eliaz, N. (2010). Electrodeposition of Zn-Ni, Zn-Fe and Zn-Ni-Fe alloys. Surf. Coat. Technol, 205, 2031–2041.

[11]. Zhang, Z., et al. (2001). Study on the behavior of Zn-Fe alloy electroplating. J. Electroanal. Chem 516, 127–130.

[12]. Bajat, J. B., Miškovic-Stankovic, V. B., & Kacarevic-Popovi, Z. (2003). The influence of steel surface modification by electrodeposited Zn-Fe alloys on the protective behaviour of an epoxy coating. Prog. Org. Coat, 47, 49–54.

[13]. Boshkov, N., Petrov, K., Kovacheva, D., Vitkova, S., & Nemska, S. (2005). Electrochim. Acta, 51, 77–84.

[14]. Bucko, M., Rogan, J., Stevanovic, S. I., Peric–Grujic, A., & Bajat, J. B. (2011). Corros. Sci., 53, 2861–2871.

[15]. Budman, E., & Sizelove, R. R. (2002). Zinc alloy plating. Metal. Finish, 100, 320-325.

[16]. Bucko, M., et al. (2013). Electrodeposition of Zn-Mn alloys at high current densities from chloride electrolyte. J. Solid State Electrochem., 17, 1409-1419.

[17]. Wu, Z., Fedrizzi, L., & Bonora, P. L. (1996). Surface and Coating Technology, 85, 170.

[18]. Abou-Krisha, M. M., Assaf, F. H., & El-Naby, S. A. (2009). Electrodeposition behavior of zinc–nickel–iron alloys from sulfate bath. J. Coat. Technol. Res., 6(3), 391–399.

[19]. Ganesan, S., Prabhu, G., & Popov, B. N. (2014). Electrodeposition and characterization of Zn-Mn coatings for corrosion protection. Surf. Coat. Technol., 238, 143-151.

[20]. Oliveira, R. P., et al. (2018). Influence of Fe^{2+} oxidation and its antioxidant ascorbic acid as additive in Zn-Ni-Fe electrodeposition process on low-carbon steel. Surface & Coatings Technology, 349, 874–884.

[21]. Abedini, B., Ahmadi, N. P., Yazdani, S., & Magagnin, L. (2020). Electrodeposition and corrosion behavior of Zn−Ni−Mn alloy coatings deposited from alkaline solution. Trans. Nonferrous Met. Soc, 30, 548-558

[22]. Lacourcelle, L. (1997). Traité de Galvanotechnique, Galva conseils edition.

[23]. Fashu, S., Khan R., & Zulfiqar, S. (2017). Ternary Zn–Mn–Sn alloy electrodeposition from an ionic liquid based on choline chloride. Transactions of the IMF, 95(4), 217-225

[24]. Rudnik, E. (2015). Effect of gluconate ions on electroreduction phenomena during manganese deposition on glassy carbon in acidic chloride and sulfate solutions. J. Electroanal. Chem, 741, 20-31.

[25]. Sylla, D., et al. (2003). Thin Solid Films, 424, 171.

[26]. Díaz-Arista, P., et al. (2009). Surf. Coat. Technol., 203, 1167–1175.

[27]. Loukil, N., & Feki, M. (2017). Synergistic effect of triton X100 and 3-hydroxybenzaldehyde on Zn-Mn electrodeposition from acidic chloride bath. Journal of Alloys and Compounds, 719, 420-428.

[28]. Casanova, T., Soto, F., Eyraud, M., & Crousier, J. (1997). Hydrogen absorption during zinc plating on steel. Corros. Sci., 39, 529-537.

[29]. Mendoza-Huízar, L. H., Rios-Reyes, C. H., & Gomez-Villegas, M. G. (2009). Zinc electrodeposition from chloride solutions onto glassy carbon electrode. J. Mex. Chem. Soc., 53(4), 243-247.

[30]. Assaf F. H., et al. (2015). Electrodeposition and Characterization of Zn-Ni-Mn Alloy from Sulfate Bath: Influence of Current Density. Int. J. Electrochem. Sci., 10, 5465-5478.

[31]. Fischer, H. (1960). Electrochim. Acta 2, 50.

[32]. Ashassi-Sorkhabi, Hagrah, H., Parvini-Ahmadi, A., & Manzoori, N. (2001). J Surf Coat Technol, 140-278.

[33]. Qiang, Y., et al. (2019). Enhanced anticorrosion performance of copper by novel N-doped carbon dots. Corrosion Science, 161, 108-193.

[34]. Nayana K. O., et al. (2019). Effect of additives on nanocrystalline bright Zn–Ni–Fe alloy electrodeposit properties. Surface Engineering, 1743-2944.

[35]. Sriramanet, K. R., et al. (2013). Characterization of corrosion resistance of electrodeposited Zn-Ni Zn and Cd coatings. Electrochim. Act, 105, 314–323.

[36]. Macdonald, J. R. (1987). Impedance Spectroscopy – Emphasizing Solid Materials and Systems, first ed., John Wiley & Sons, New York.

[37]. Hegde, A. C., Venkatakrishna, K., & Eliaz, N. (2010). Electrodeposition of Zn–Ni, Zn–Fe and Zn–Ni–Fe alloys. Surface & Coatings Technology, 205, 2031–2041.

[38]. Hall, D. E. (1983). Plat. Surf. Finish. 71, 59.

[39]. Brenner, A. (1963). Volumes I and II, Academic Press, New York.

[40]. Elkhatabi, F., Sarret M., & Muller, C. (1996). J. Electroanal. Chem., 404, 45.